Aerosp. Sci. Technol. 4 (2000) 41–55

S1270-9638(00)00114-0/FLA

A Dynamic Finite Element (DFE) method for free vibrations of bending-torsion coupled beams

S. Mohammad Hashemi [a], Marc J. Richard [a,*]

[a] Department of Mechanical Engineering, Laval University Québec, Québec G1K 7P4, Canada

Received 22 December 1998; revised 5 December 1999; accepted 6 December 1999

Abstract

In this paper, a Dynamic Finite Element (DFE) formulation for the free vibration analysis of bending-torsion coupled beams is presented. First, the exact solutions of the differential equations governing the uncoupled vibrations of a uniform beam are found. The employment of these solutions as basis functions leads to the appropriate frequency dependent shape functions which can then be utilized to find the nodal approximations of variables. By exploiting the Principle of Virtual Work (PVW), the elementary Dynamic Stiffness Matrix (DSM) is then obtained which has both mass and stiffness properties. The implementation of the derived DFE matrices in a program is discussed with a particular reference to the Wittrick–Williams algorithm. The application of the theory is demonstrated by illustrative examples wherein a substantial amount of coupling between bending and torsion is highlighted. The correctness of the theory is confirmed, to a high degree of accuracy, by published results and numerical checks. © 2000 Éditions scientifiques et médicales Elsevier SAS

coupled bending-torsion vibration / Dynamic Finite Element / beam

Nomenclature

D_f	denominator in the expressions of flexural shape functions (N_{if}; $i = 1, 2, 3, 4$)
D_t	denominator in the expressions of N_{1t} and N_{2t} (torsional shape functions)
$\Delta = D_f * D_t$	denominator in $[K_{DS}]^k$
$H_f = EI$	Flexural Rigidity
$H_t = GJ$	Torsional Rigidity
$[K_{DS}]$	overall dynamic stiffness matrix
$[K_{DS}^{\Delta}]$	upper triangular matrix obtained from K_{DS}
$[K_{DS}]^k$	element stiffness matrix
$[K_{DS}]^k_{\text{Uncoupl}}$	first part of $[K_{DS}]^k$ corresponding to the uniform beam element "k"
$[K_{DS}]^k_{\text{Coupl}}$	the coupling part of $[K_{DS}]^k$
$(K_C)^k_{ij}$	components of $[K_{DS}]^k_{\text{Coupl}}$; $i = 1, 2$; $j = 1, 2, 3, 4$
L	total length of the beam
NE	total number of elements
$\mathcal{W}$	total virtual work
$\mathcal{W}_{INT}$	internal virtual work
$\mathcal{W}_{EXT}$	external virtual work
$\mathcal{W}^k$	discretized virtual work due to "k"th element
$\mathcal{W}^k_f$	the bending part of W^k
$\mathcal{W}^k_t$	the torsion part of W^k
l_k	the length of element "k"
$m = \rho A$	mass per unit length
w	flexural displacement
W	amplitude of the flexural displacement
δW	test function due to the bending
ψ	torsional rotation
Ψ	amplitude of the torsional rotation; ($\Psi \equiv Psi$)
$\delta\Psi$	test function due to the torsion
x_α	distance between the mass and the elastic axes
$\xi = s/l_k$	elementary local coordinate, $0 \leqslant \xi \leqslant 1$
ω	rotary frequency; ($\omega \equiv omega$)

* Correspondence and reprints

1. Introduction

The vibration of a straight uniform beam for which the elastic or flexural axis is not coincident with the inertial axis is characterized by a combination of bending translation and torsional rotation. Many engineering structures exhibit this type of motion. Aircraft wings and control surfaces and also turbine, helicopter and propeller blades of high aspect ratio, all qualify (at least for their first few vibration modes) as beams which usually have non-coincident elastic and inertial axes [14]. Naturally, it is very important to take into account the coupling effects in vibration and response calculations of structures made up of these beams. This is particularly so for aeroelastic problems; for example, coupled bending-torsional modes are often required for flutter analysis of an aircraft wing [2]. Moreover, some complete aircraft structures can be represented with reasonable accuracy as assemblages of such beams connected together [14].

Because of the practical importance of coupled bending-torsion beam vibrations, many approaches for the calculation of vibration modes have been exploited. For approximate solutions one may discretize by either the lumped-mass method [2,20] or one of the methods based on the assumed deformation shapes. The latter category includes the Rayleigh–Ritz method [20,9], the Galerkin method [12], and the Finite Element Method (FEM) [21] where beam element matrices are evaluated from assumed fixed shape functions (like polynomials). A generalized linear eigenvalue problem then results. The Dynamic Stiffness Matrix (DSM) method probably offers a better alternative, particularly when higher frequencies and better accuracies of results are required. It relies on only one frequency dependent matrix which has both mass and stiffness properties of the element combined, embedded into it. The use of a DSM in vibration analysis is well established [23,24,1]. Obviously the method gives more accurate results because it exploits the exact member theory. The matrix is obtained by directly solving the governing differential equation and hence all assumptions, being within the limits of the differential equations only, are less severe. Hence, the results obtained by using a DSM are often justifiably called "exact" [3] (when the differential equation can be solved exactly). A generalized nonlinear eigenvalue problem then results. But it implies, sometimes, mathematical procedures which are difficult to deal with, and/or are often limited to special cases.

The Dynamic Finite Element (DFE) approach developed here produces the accurate solutions for coupled flexural-torsional vibration of beams, and of structures composed of such beam elements. This method can be considered as a combination of two methods. First the well known "weighted residual method" procedure, as in the FEM, is adopted to provide a general tool, and secondly the advantages of the DSM method are retained by choosing the weighting functions, shape functions, etc, referring to the appropriate exact uncoupled member equations. The eigenvalue problem resulting from this method, is also a nonlinear one. The DFE approach can be extended to more complex cases which distinguishes this method from the DSM method. The dynamic finite element for coupled bending-torsional vibration of a beam is developed from the basic differential equations of motion. The method of incorporating the derived stiffness expressions in a computer program for vibration analysis of beams, and of structures composed of beams, having a non-coincident shear centre and mass centre is discussed. The application of the theory is demonstrated by results obtained for illustrative examples of an open-box cross-section and the wings of different configurations wherein a substantial amount of coupling between bending and torsion is highlighted. Numerical checks are performed to confirm the predictable accuracy and to ensure confidence for practical applicability of the theory.

2. Mathematical model

A uniform beam of length L is shown in *figure 1* with the mass axis and the elastic axis (which are respectively the loci of the mass centre and the shear centre of the cross-sections) being separated by a distance x_α. In the right handed coordinate system shown in *figure 1*, the elastic axis, which is assumed, as is customary in aerospace structures studies, to be coincident with the y-axis, is permitted flexural translation $w(y,t)$ in the z-direction and torsional rotation $\psi(y,t)$ about the y-axis where y and t denote distance from the origin and time respectively.

Using the Bernoulli–St-Venant beam theory (i.e., neglecting the shear deformation, rotary inertia and warping of the cross-section), the governing partial differential equations of motion of the beam, shown in *figure 1*, are given by [12]

$$H_f w'''' + m\ddot{w} - mx_\alpha \ddot{\psi} = 0, \tag{1}$$

$$H_t \psi'' - I_\alpha \ddot{\psi} + mx_\alpha \ddot{w} = 0, \tag{2}$$

with appropriate boundary conditions imposed at $y = 0, L$. H_f and H_t are respectively the bending and torsional rigidity of the beam; m is the mass per unit length, I_α is the polar mass moment of inertia per unit length about the y-axis (i.e., an axis through the shear centre), t represents time and the primes and dots denote differentiation with respect to position y and t, respectively.

For the free vibration analysis, a sinusoidal variation of w and ψ, with circular frequency ω, is assumed

$$w(y,t) = W(y)\sin(\omega t),$$

$$\psi(y,t) = \Psi(y)\sin(\omega t), \tag{3}$$

where $W(y)$ and $\Psi(y)$ are the amplitudes of the sinusoidally varying vertical displacement and torsional rotation, respectively.

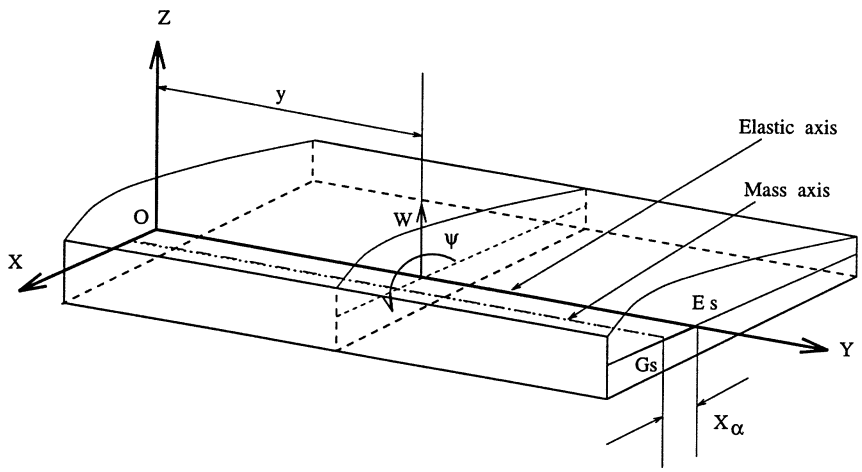

Figure 1. Coordinate system and notations for coupled bending-torsional vibration of a uniform beam element: E_s shear centre; G_s mass centre.

Substituting equations (3) into (1) and (2) gives

$$H_f W'''' - m\omega^2 W + m x_\alpha \omega^2 \Psi = 0, \tag{4}$$

$$H_t \Psi'' + I_\alpha \omega^2 \Psi - m x_\alpha \omega^2 W = 0. \tag{5}$$

The integral form associated to equations (1) and (2) is then written as:

$$\mathcal{W}_f = \int_0^L \delta W \left\{ (H_f) W'''' - \left(m\omega^2\right) W + \left(m x_\alpha \omega^2\right) \Psi \right\} \mathrm{d}y, \tag{6}$$

$$\mathcal{W}_t = \int_0^L \delta \Psi \left\{ -(H_t) \Psi'' + \left(I_\alpha \omega^2\right) \Psi - \left(m x_\alpha \omega^2\right) W \right\} \mathrm{d}y. \tag{7}$$

Here, W and Ψ are solution functions and δW and $\delta \Psi$ are test functions. Then, applying an appropriate number of integrations by parts allows us to diminish the derivatives order and the Galerkin type weak form associated to equations (1) and (2) is obtained as:

$$\mathcal{W}_f = \int_0^L \left\{ (H_f) \delta W'' W'' - \left(m\omega^2\right) \delta W W + \left(m x_\alpha \omega^2\right) \delta W \Psi \right\} \mathrm{d}y + \left[(H_f) \left(\delta W W''' - \delta W' W'' \right) \right]_0^L, \tag{8}$$

$$\mathcal{W}_t = \int_0^L \left\{ -(H_t) \delta \Psi' \Psi' + \left(I_\alpha \omega^2\right) \delta \Psi \Psi - \left(m x_\alpha \omega^2\right) * \delta \Psi W \right\} \mathrm{d}y + \left[\delta \Psi H_t \Psi' \right]_0^L, \tag{9}$$

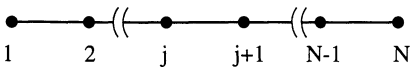

Figure 2. The domain, discretized by a number of 2-node elements.

where both solution and test functions are defined in the same approximation space. For Clamped-Free boundary conditions, for example, it is assumed that

$$\delta W = \delta W' = \delta \Psi = 0 \quad \text{at } y = 0,$$

and force terms are zero at $y = L$. Consequently, the boundary terms in the above expressions will disappear. However, it can be verified that also for any other boundary conditions, similar results can be obtained when the proper constraints are applied regarding test functions. Expressions (8) and (9) also satisfy the Principle of Virtual Work (PVW)

$$\mathcal{W} = \mathcal{W}_{INT} - \mathcal{W}_{EXT} = 0,$$

where

$$\mathcal{W}_{INT} = \mathcal{W}_f + \mathcal{W}_t, \tag{10}$$

and $\mathcal{W}_{EXT} = 0$, for free vibrations.

If the domain is discretized by a number of 2-node elements [10], we have (see *figure 2*):

$$\mathcal{W} = \mathcal{W}_{INT} = \sum_{k=1}^{NE} \mathcal{W}^k, \tag{11}$$

where

$$\mathcal{W}^k = \mathcal{W}_f^k + \mathcal{W}_t^k; \tag{12}$$

and

$$\mathcal{W}_f^k = \int_{y_j}^{y_{j+1}} \left\{(H_f)\delta W'' W'' - \left(m\omega^2\right)\delta W W\right\} \mathrm{d}y + \int_{y_j}^{y_{j+1}} \left(mx_\alpha\omega^2\right)\delta W \Psi \,\mathrm{d}y, \tag{13}$$

$$\mathcal{W}_t^k = \int_{y_j}^{y_{j+1}} \left\{-(H_t)\delta\Psi'\Psi' + \left(I_\alpha\omega^2\right)\delta\Psi\Psi\right\} \mathrm{d}y - \int_{y_j}^{y_{j+1}} \left(mx_\alpha\omega^2\right)\delta\Psi W \,\mathrm{d}y. \tag{14}$$

Each element is defined by nodes $j, j+1$ with corresponding coordinates.

The components of $\mathcal{W}^k$ may also be written in an equivalent form obtained after integration by parts on each element:

$$\mathcal{W}_f^k = \int_{y_j}^{y_{j+1}} W\left\{(H_f)\delta W'''' - \left(m\omega^2\right)\delta W\right\} \mathrm{d}y + \left[(H_f)\left\{\delta W'' W' - \delta W''' W\right\}\right]_{y_j}^{y_{j+1}} + \int_{y_j}^{y_{j+1}} \left(mx_\alpha\omega^2\right)\delta W \Psi \,\mathrm{d}y, \tag{15}$$

$$\mathcal{W}_t^k = \int_{y_j}^{y_{j+1}} -\Psi\left\{(H_t)\delta\Psi'' + \left(I_\alpha\omega^2\right)\delta\Psi\right\} \mathrm{d}y + \left[(H_t)\delta\Psi'\Psi\right]_{y_j}^{y_{j+1}} + \int_{y_j}^{y_{j+1}} \left(mx_\alpha\omega^2\right)\delta\Psi W \,\mathrm{d}y. \tag{16}$$

The admissibility condition for the finite element approximation is controlled by equations (8) and (9). The approximation for $W, \delta W$ is of C^1-type, assuring continuity of W and $W_{,x}$ at each node, and the approximation for $\Psi, \delta\Psi$ is of C^0-type. Equations (15) and (16) present simply another way of evaluating equations (8) and (9) at the element level.

2.1. Finite Element (FE) formulation

The classical Finite Element (FE) model is found by using Hermite type polynomial approximation such as

$$W(x) = N_1(x)W_1 + N_2(x)W_1' + N_3(x)W_2 + N_4(x)W_2', \tag{17}$$

where W_1 and W_2 are nodal values at node j, $j+1$, corresponding to out-of-plane (flapping) flexural displacements. For torsional displacement $\Psi(x)$, in this case, one uses the linear approximation. Identical approximation is chosen for δW and $\delta\Psi$, respectively. The discretized representation of equations (10) is then obtained as:

$$\mathcal{W} = \sum_{k=1}^{NE} \mathcal{W}^k = \left([K] - \lambda[M]\right)\{w_n\} = 0. \tag{18}$$

This is a classical linear eigenvalue problem which is solved using an inverse iteration procedure, subspace or Lanczos method [6].

2.2. Exact Dynamic Rigidity method

Let us consider the case of a uniform coupled beam for which all parameters (H_f, H_t, $m(x)$, etc.) are constant over the element. Under these circumstances it is possible to write down a general solution for W and Ψ which leads to an Exact Dynamic Stiffness Matrix (DSM) [2]. However, when coefficients H_f, H_t, $m(x)$, etc. are not constant, it will not be possible to calculate the DSM in this way and the application of this method will be limited to special cases.

2.3. Dynamic Finite Element (DFE) method

In this study, we propose an intermediate approach in which, the classical Finite Elements Method (FEM) is combined to the Dynamic Stiffness Matrix (DSM) approach, to obtain a better finite element model. The approximation space is defined by frequency dependent hyperbolic functions and the appropriate interpolation functions are obtained with averaged value parameters over each element. The solutions of the uncoupled form of the governing differential equations of motion are utilized, as expansion terms, to find the shape functions. Then, these shape functions, all being frequency dependent, can be used to obtain the corresponding stiffness matrix. In this paper, the DFE method is developed and demonstrated for the case of a "uniform coupled beam" where the coefficients H_f, H_t, $m(x)$, etc. are constant. But the advantage of the DFE methodology, comparing to the DSM approach, is that it can be extended to more complex cases as coupled beams with variable geometry and properties. To this end, the interesting features of the DFE methodology presented in the earlier works of the authors, can be exploited (see for example [16,17,19]).

To obtain the DFE method formulation, equations (15) and (16) are rearranged in the following form which present simply another method to evaluate equations (8) and (9) at the element level (see *figure 3*):

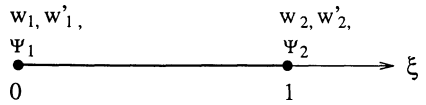

Figure 3. The 2-node reference element.

$$\mathcal{W}_f^k = \int_0^1 W \underbrace{\left\{ \frac{H_f}{l_k^3}\delta W'''' - \left(ml_k\omega^2\right)\delta W \right\}}_{*} \mathrm{d}\xi + \left[\left(\frac{H_f}{l_k^3} \right) \left\{ \delta W'' W' - \delta W''' W \right\} \right]_0^1 + \int_0^1 \left(ml_k x_\alpha \omega^2\right)\delta W \Psi \, \mathrm{d}\xi, \tag{19}$$

$$\mathcal{W}_t^k = \int_0^1 -\Psi \underbrace{\left\{ \frac{H_t}{l_k}\delta\Psi'' + \left(I_\alpha l_k\omega^2\right)\delta\Psi \right\}}_{**} \mathrm{d}\xi + \left[\left(\frac{H_t}{l_k} \right) \delta\Psi' \Psi \right]_0^1 + \int_0^1 \left(ml_k x_\alpha \omega^2\right)\delta\Psi W \, \mathrm{d}\xi, \tag{20}$$

where $\xi = y/l_k$.

Then, the approximations are made for δW, W, $\delta\Psi$ and Ψ so that $(*)$ and $(**)$ vanish:

$$\delta W = \langle P(\xi)\rangle_f * \{\delta a\}; \quad W = \langle P(\xi)\rangle_f * \{a\}, \tag{21}$$

$$\delta\Psi = \langle P(\xi)\rangle_t * \{\delta b\}; \quad \Psi = \langle P(\xi)\rangle_t * \{b\}, \tag{22}$$

where

$$\langle P(\xi)\rangle_f = \left\langle \cos(\alpha\xi);\ \frac{\sin(\alpha\xi)}{\alpha};\ \frac{\cosh(\alpha\xi) - \cos(\alpha\xi)}{\alpha^2};\ \frac{\sinh(\alpha\xi) - \sin(\alpha\xi)}{\alpha^3} \right\rangle, \tag{23}$$

$$\langle P(\xi)\rangle_t = \left\langle \cos(\tau\xi);\ \frac{\sin(\tau\xi)}{\tau} \right\rangle \tag{24}$$

and

$$\alpha = l_k \sqrt{\omega \sqrt{\frac{m}{H_f}}}; \qquad \tau = \sqrt{\frac{I_\alpha\, \omega^2}{H_t}}. \tag{25}$$

Considering $\langle \delta a\rangle$ and $\langle \delta b\rangle$ as nodal variables $\langle W_1; W_1'; W_2; W_2'\rangle$, $\langle \Psi_1; \Psi_2\rangle$, respectively, we obtain

$$\{\delta W_n\} = [P_n]_f * \{\delta a\}, \tag{26}$$

$$\{\delta\Psi_n\} = [P_n]_t * \{\delta b\} \tag{27}$$

and hence the approximations (21) and (22) in nodal variables are written as:

$$W(\xi) = \langle P(\xi)\rangle_f [P_n]_f^{-1}\{W_n\} = \langle N(\xi)\rangle_f \{W_n\}, \tag{28}$$

$$\Psi(\xi) = \langle P(\xi)\rangle_t [P_n]_t^{-1}\{\Psi_n\} = \langle N(\xi)\rangle_t \{\Psi_n\} \tag{29}$$

and can be rearranged as:

$$\begin{Bmatrix} W(\xi) \\ \Psi(\xi) \end{Bmatrix} = [N] * \{w_n\}, \tag{30}$$

where

$$\{w_n\} = \left\langle W_1 W_1' \Psi_1 W_2 W_2' \Psi_2 \right\rangle^T \tag{31}$$

and

$$[N] = \begin{Bmatrix} \langle N_f\rangle \\ \langle N_t\rangle \end{Bmatrix} \tag{32}$$

$$= \begin{bmatrix} N_1(\omega)_f & N_2(\omega)_f & 0 & N_3(\omega)_f & N_4(\omega)_f & 0 \\ 0 & 0 & N_1(\omega)_t & 0 & 0 & N_2(\omega)_f \end{bmatrix}$$

are the frequency dependent dynamic shape functions, mentioned earlier. Equations (A)–(H) of the Appendix represent, respectively, the bending dynamic shape functions (i.e., $N_i(\omega)_f;\ i = 1, 2, 3, 4$), and those due to the uncoupled torsional vibrations (i.e., $N_i(\omega)_t;\ i = 1, 2$).

Then, using the approximation functions mentioned above, the Dynamic Finite Element model becomes:

$$\mathcal{W}_f^k = \left[\left(\frac{H_f}{l_k^3} \right) \left\{ \delta W'' W' - \delta W''' W \right\} \right]_0^1 + \int_0^1 \left(ml_k x_\alpha \omega^2\right)\delta W \Psi \, \mathrm{d}\xi, \tag{33}$$

$$\mathcal{W}_t^k = \left[\left(\frac{H_t}{l_k} \right) \delta\Psi' \Psi \right]_0^1 + \int_0^1 \left(ml_k x_\alpha \omega^2\right)\delta\Psi W \, \mathrm{d}\xi \tag{34}$$

which leads to the following matrix form;

$$\mathcal{W}^k = \langle \delta w_n\rangle [K_{DS}]^k \{w_n\}. \tag{35}$$

Here, the DFE stiffness matrix can be represented as:

$$[K_{DS}]^k = [K_{DS}]^k_{\text{Uncoupl}} + [K_{DS}]^k_{\text{Coupl}} \tag{36}$$

in which

$$[K_{DS}]^k_{\text{Uncoupl}} = \Big[\underbrace{c_f\{N_f'''\};\ c_f\{-N_f''\};\ c_t\{-N_t'\}}_{\xi=0}; \underbrace{c_f\{-N_f'''\};\ c_f\{N_f''\};\ c_t\{N_t'\}}_{\xi=1} \Big], \tag{37}$$

$$[K_{DS}]^k_{\text{Coupl}} = \left(m x_\alpha l_k \omega^2\right) \tag{38}$$

$$\times \begin{bmatrix} 0 & 0 & (Kc)_{11} & 0 & 0 & (Kc)_{21} \\ & 0 & (Kc)_{12} & 0 & 0 & (Kc)_{22} \\ & & 0 & (Kc)_{13} & (Kc)_{14} & 0 \\ & & & 0 & 0 & (Kc)_{23} \\ & \textit{Sym.} & & & 0 & (Kc)_{24} \\ & & & & & 0 \end{bmatrix},$$

where

$$(Kc)_{ij} = \int_0^1 N_{it} \cdot N_{jf} \cdot \mathrm{d}\xi \begin{cases} i = 1, 2, \\ j = 1, 2, 3, 4, \end{cases} \tag{39}$$

and $c_f = H_f / l_k^3$; $c_t = H_t / l_k$.

It can be readily verified from equations (35) through (39) that the second term in equation (35), representing the coupling between flexural and torsional vibrations of the beam element, reduces to zero when $x_\alpha = 0$ ($x_\alpha = 0$ can be substituted in the derived expressions without causing any overflow or underflow). Thus, the degenerated stiffness matrix of equation (35) becomes the 'exact' stiffness matrix representing the uncoupled flexural and torsional vibrations of an Euler–Bernoulli beam element [24,25]. It can be also verified that when $\omega \to 0$, the functions of equations (23) and (24) become; $1; x; x^2; x^3$; and $1; x$, respectively. The former, represent the expansion terms (or basis functions) in the conventional finite beam element formulation, when the nodal approximation of the flexural degrees of freedom are expressed by using the cubic "Hermite" type polynomial interpolation functions. The latter, are usually used as the basis functions leading to the well-known linear polynomial shape functions (for example, to study the torsion in the standard finite beam element formulation). In this case, the shape functions of equations (A)–(H) of the Appendix become the corresponding shape functions actually used in the static conventional FEM. Therefore, the dynamic stiffness matrix of equation (35) changes to a static stiffness matrix of a "Hermite" type beam element, when the torsion is also included by using a linear approximation approach [10].

One notes that the derivation of the stiffness expressions given by equations (35) through (38) relate to flexure in the y–z plane (see *figure 1*). However, the x–y plane could have been chosen instead, in which case, care must be taken to substitute appropriate values of the bending rigidity (H_f) and the distance between the shear centre and the mass centre (x_α). Using this approach to find the stiffness expressions corresponding to both planes, a 12×12 dynamic stiffness matrix of the beam element in three dimensions can be constructed to enable vibration analysis of space frames which incorporate such members.

3. Application of the theory

The expressions for the DFE stiffness matrix, $[K_{DS}]^k$, derived in the previous section can be directly used to compute the natural frequencies of coupled bending-torsion vibrations of beams and the assemblage of bending- torsion coupled beams. Elementary matrices then will have to be assembled in the usual way to form the overall dynamic stiffness matrix $[K_{DS}]$ of the final structure. The eigenvalue problem resulting from this method, for free vibrations, is found then to be:

$$[K_{DS}] * \{W_n\} = \{0\} \tag{40}$$

which is a nonlinear one. The determination of the natural frequency then follows from equation (40) and the well-known Wittrick–Williams algorithm described on several occasions in the literature (e.g., see [23,24,1,22]).

According to the Wittrick–Williams algorithm [22], the following features of the solution are important:

(a) $|K_{DS}| = 0$, $\{W_n\} \neq 0$ is one set of solutions,

(b) $|K_{DS}| = \infty$, $\{W_n\} = 0$ is not necessarily a trivial set of solutions, but corresponds to the case where the displacements $\{W_n\}$ happen to correspond to nodes of some of the natural modes of vibration of the system. It can be seen from equation (40) that the natural frequencies of the constrained system in general correspond to $|{K_{DS}}^{-1}| = 0$, which in turn implies that $|K_{DS}| = \infty$. The procedure is briefly summarized as follows.

Suppose that ω denotes the circular frequency of the beam. Then it is known that j, the number of eigenvalues passed as ω is increased from zero to ω^*, is given by

$$j = j_0 + s\{K_{DS}\}, \tag{41}$$

where $[K_{DS}]$ is the overall DSM (which is ω dependent) of the structure, evaluated at $\omega = \omega^*$; $s\{K_{DS}\}$ is the number of negative elements on the leading diagonal of K^{Δ}_{DS}, K^{Δ}_{DS} is the upper triangular matrix obtained by applying the usual form of Gauss elimination to K_{DS} and j_0 is the number of natural frequencies of the beam still lying between $\omega = 0$ and $\omega = \omega^*$ when the displacement components to which K_{DS} corresponds are all zero (the beam can still have natural frequencies when all its nodes are clamped, because the formulation presented allows each individual element to have an infinite number of degrees of freedom between nodes). Thus

$$j_0 = \sum_{m=1}^{EN} j_m, \tag{42}$$

where j_m is the number of natural frequencies between $\omega = 0$ and $\omega = \omega^*$ for an element with its ends clamped, while the summation extends over all the elements.

For the element stiffness matrix developed in this paper, the constrained frequencies of an individual element

occur when one or more of the components of the matrices of equations (37) and (38) become infinite (i.e., $\Delta = D_f * D_t = 0$). This will occur when $D_f = 0$ or $D_t = 0$, where D_f and D_t are, respectively, the denominators in flexural and torsional dynamic shape functions, given in expressions in the Appendix. Numerous standard texts show that when

$$D_f = 0 \tag{43}$$

this gives the natural frequencies of flexural vibrations of a uniform clamped-clamped beam, and it is easily verified that the number of these natural frequencies lying between zero and any trial ω is given [24] by

$$j_f = i - \frac{1}{2}\left[1 - (-1)^i \operatorname{sgn}\{D_f\}\right];$$
$$i = \text{largest integer} < \frac{\alpha}{\pi} \tag{44}$$

in which $\operatorname{sgn}\{D_f\} = 1$ when D_f is positive, and is -1 when D_f is negative. The equation

$$D_t = 0 \tag{45}$$

represents the natural frequencies of torsional vibrations of a uniform clamped-clamped beam [25], and the number of these natural frequencies exceeded by any trial ω is given by

$$j_t = \text{the highest integer} < \frac{\tau}{\pi}. \tag{46}$$

α and τ are calculated from expressions (25). Hence

$$j_m = j_f + j_t \tag{47}$$

Then, j_0 follows from equation (42).

Thus, exploiting the relations in equations (41) through (47), it is possible to converge on any required natural frequency, given the fact that the expressions for the DFE stiffness matrix and the clamped-clamped natural frequencies are known. Then, the mode shapes are calculated by using equation (40).

The j_0's value was also calculated based on the method presented in reference [5] (see also [15]). The procedure explained here is implemented in the so-called RE-FLEX [7] conventional FEM computer program to obtain the results given in the next section, when the integral terms of equation (39) are evaluated by using 12 integration points.

4. Numerical tests

Numerical checks are performed to confirm a good accuracy and to ensure confidence for practical applicability and the performance of the theory. In what follows, based on the theory of this paper, some examples of different configurations of beam assemblies are presented.

First, the numerical results were obtained for a thin-walled open section beam given by Banerjee [2]. The aim of the authors to present this example is to demonstrate the validity of the proposed method for evaluating j_m (i.e., the number of natural frequencies between $\omega = 0$ and $\omega = \omega^*$ for an element with its ends clamped). Moreover, the application of the DFE approach to the free vibrational analysis of the open section coupled beams with different boundary conditions, is also investigated. Then, numerical tests were carried out for a group of cantilever closed section beam-like wings and very good agreement was found between the results obtained by the DFE approach and those existing in the literature.

Furthermore, it was also confirmed that substituting $x_\alpha = 0$ in the DFE expressions, leads to the exact solutions of uncoupled flexural and torsional natural frequencies of Euler–Bernoulli and the St-Venant beams, respectively [24,25].

4.1. Thin-walled open box section

A cantilever beam of aluminum material and of length 5 m with the cross section of a thin-walled open box section shown in *figure 4* is considered [2]. Note that the small cut in the section reduces the torsional rigidity quite drastically whereas the bending rigidity is virtually unaltered. The distance of the shear centre from the centroid (x_α) and the Saint Venant torsional constant (J) of the section were experimentally established [2] at 0.08 m and 2.69×10^{-9} m^4, respectively. Thus these experimental values and the values given for the Bending rigidity (H_f), torsional rigidity (H_t), mass per unit length (m), polar mass moment of inertia per unit length about an axis

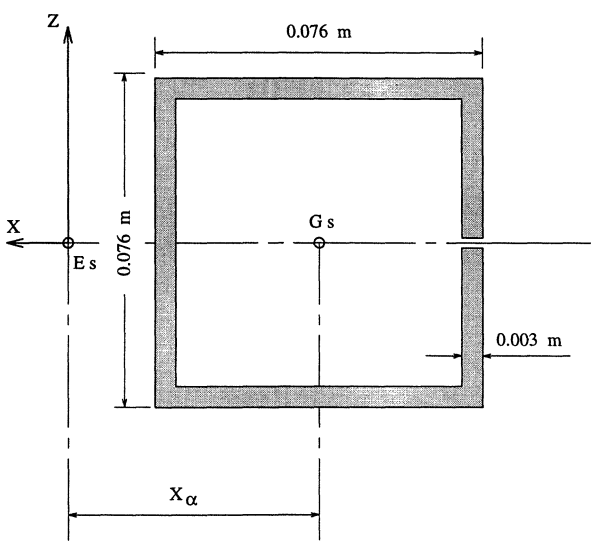

Figure 4. Sectional details of an open box beam: E_s shear centre: G_s mass centre.

Table I. Coupled bending-torsional C-C natural frequencies of an open box.

	Frequency f_i (Hz)					
i	Exact	DFE[a]	DFE	Approx.	FEM[b]	FEM[c]
1	6.07	6.07	6.07	6.06	6.07	6.07
2	12.32	12.32	12.32	12.26	12.37	12.36
3	18.45	18.48	18.48	18.28	18.63	18.62
4	24.81	24.82	24.82	24.40	25.23	25.22
5	31.07	31.12	31.12	30.27	31.89	31.86

[a] The number of C-C natural frequencies, layed between a trial frequency and zero, in this case, are found by an exact method, see reference [5].

[b] To find these results, a total of 20 classical beam elements [8] are used.

[c] To find these results, a total of 20 classical beam elements [14] are used.

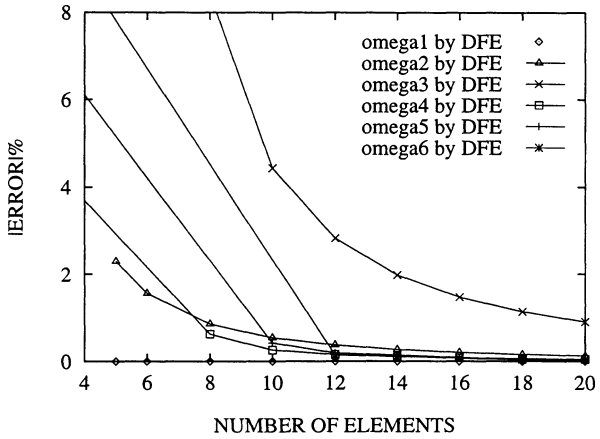

Figure 5. Convergency test for the first three natural frequencies of the clamped-free (C-F) beam.

through the shear centre from the centroid (I_α) and the distance of the shear centre from the centroid (x_α) were, respectively, 5.8×10^4 N·m^2, 78.3 N·m^2, 2.45 kg/m, 0.02 kg·m and 0.08 m. The natural frequencies (ω_i) are calculated from the DFE method for the cantilever beam. A direct comparison was made between the results obtained by the DFE and the exact results and also the approximated results found by using lumped masses and inertias. In this case, the results presented by Banerjee [2] were used.

The first five natural frequencies in Hertz (f_i, $i = 1, 2, \ldots, 5$) for clamped-clamped (C-C) end conditions obtained from this approximate analysis, as well as exact results, are given in *table I* together with the results obtained from the conventional Finite Elements (FEM) and the DFE method.

The "exact" results, presented in *table I* were obtained by the explicit expressions for the coupled dynamic stiffness matrix of a uniform beam element, derived in an exact sense by solving the governing differential equation of the beam.

The approximate results have been obtained for $N = 20$ (the number of lumped parameters). The results obtained by this approach, for the first three C-C natural frequencies, were converging between $N = 20$ and $N = 25$ with less than one percent error [2].

The conventional FEM's results were obtained using a total of 20 classical beam elements and two types of elements were used. First, the beam element presented in reference [8] was exploited in which the mass matrix was obtained by using the linear approximations for all variables. Secondly, the tests were repeated with the beam element presented in reference [14]. The mass matrix, in this case, was obtained by using the cubic "Hermite" type and linear approximations for bending and torsion, respectively. The static stiffness matrix, in both cases, was also found by using the cubic "Hermite"

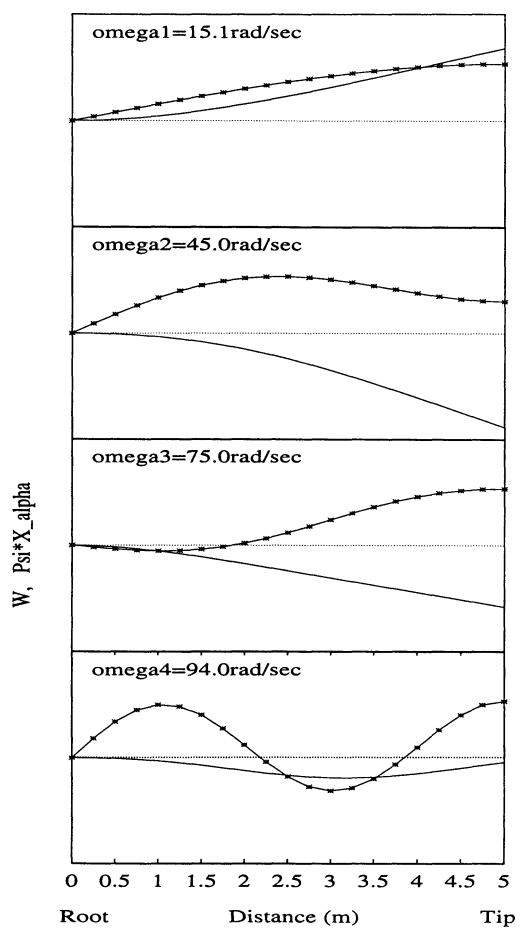

Figure 6. The coupled bending-torsional natural frequencies and modes of an open box beam. ——, flexural displacement (W); —∗—, torsional displacement ($\Psi * x_\alpha$).

type and linear approximations for flexural and torsional displacements, respectively. Comparing these results to those obtained from the lumped parameters analysis one observes approximately the same size errors, but the latter element leads to slightly better rates of convergence compared to the former one.

The results obtained by the DFE method, were calculated by two methods. First, j_m (the number of C-C natural frequencies, of bending-torsion coupled beam element, lying between zero and any trial ω), was calculated by the method of reference [5]. Then, j_m was calculated by the method presented in this paper ($\Delta = D_f * D_t = 0$ see equations (42) through (47)). The same results (difference $\leqslant 0.001$), for the C-C natural frequencies, are obtained by both methods, when $NE = (i + 1)$ elements were used to find the ith C-C natural frequency. To find the first five C-C natural frequencies, only six elements are used ($NE = 6$), and the errors were found to be less than 0.2%.

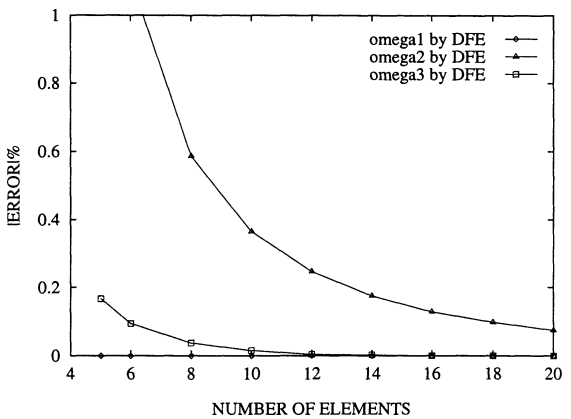

Figure 7. Convergency test for the first three natural frequencies of the Simply Supported (S-S) beam. Rigid body modes in this case are discounted.

As it can be seen from *table I*, the DFE methodology, compared to the FEM, provides excellent results with much better convergency rates.

The convergency tests, for the first six clamped-free natural frequencies, obtained by the DFE method are presented in *figure 5*. As it can be seen for the first natural frequency the error is found to be approximately zero ($\varepsilon \leqslant 0.1\%$), even when only five elements are used. For the second natural frequency, the results are converging between $NE = 6$ and $NE = 8$ with less than 1 percent error, and the significant results for the fourth, fifth and sixth natural frequencies, respectively, are obtained when the beam is discretized by 8, 10, and 12 elements. For the third natural frequency, an error less than 1 percent was found for *NE* less than 20. The coupled clamped-free natural frequencies and modes of this example are shown in *figure 6*. *Figure 7* shows the convergency tests, for simply supported natural frequencies. The natural frequencies are well separated, but the generated modes show a substantial coupling between flexural and torsional rotations.

4.2. Application to a typical uniform aircraft wing

As the second example, the natural frequencies and mode shapes of a typical cantilever uniform aircraft wing [13,11] are investigated. The flexural and torsional motion, in this case, are coupled and the wing is defined by the following data:

(i) bending rigidity $(EI) = 9.75$ MN·m^2;
(ii) torsional rigidity $(GJ) = 0.988$ MN·m^2;
(iii) mass per unit length $(m) = 35.75$ kg/m;
(iv) mass moment of inertia per unit length $(I_\alpha) = 8.65$ kg·m;

Table II. Coupled bending-torsional natural frequencies of a typical cantilever wing.

	Frequency f_i [rad/sec]						
i	Exact[a]	DFE[b]	$\lvert\text{Err.}_{(c)}\rvert$	FEM[c]	$\lvert\text{Err.}_{(c)}\rvert$	FEM[d]	$\lvert\text{Err.}_{(d)}\rvert$
1	49.62	49.62	0.00(%)	49.56	0.12(%)	49.62	0.00(%)
2	97.04	97.05	0.01(%)	97.00	0.04(%)	97.04	0.00(%)
3	248.87	249.00	0.05(%)	248.61	0.11(%)	248.88	0.04(%)
4	355.59	357.54	0.55(%)	352.97	0.74(%)	355.59	0.00(%)
5	451.46	452.57	0.25(%)	450.89	0.13(%)	451.48	0.004(%)
6	610.32	610.63	0.05(%)	610.18	0.02(%)	610.39	0.01(%)

[a] The "exact" results obtained from the DSM method presented in reference [2] .
[b] The natural frequencies calculated by DFE, when only six elements are used.
[c] The results obtained from the classical FEM when the wing is broken into 200 static beam elements of reference [8].
[d] The results obtained from the classical FEM when the wing is broken into 200 static beam elements of reference [14].

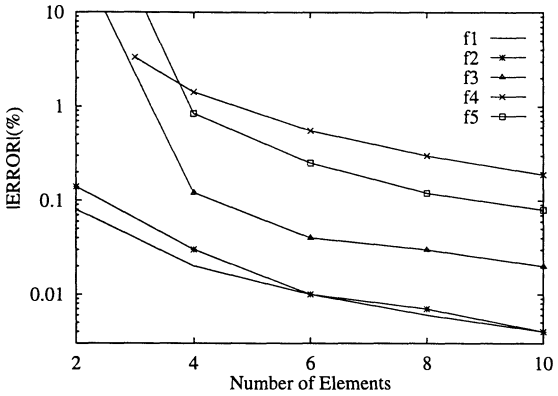

Figure 8. Convergency test for the first five natural frequencies of the cantilever uniform wing.

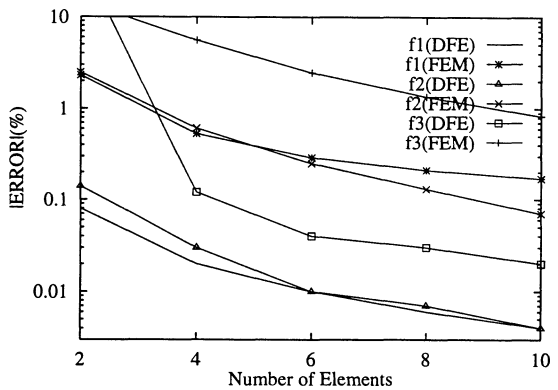

Figure 9. Convergency rates comparison for the first three natural frequencies of the cantilever uniform wing by DFE and FE methods.

(v) distance between mass centre and shear centre $(x_\alpha) = 0.18$ m;

(vi) length of the wing $(L) = 6$ m.

The Clamped-Free (C-F) natural frequencies (f_i) are calculated from the DFE method for this wing, and a direct comparison was made between these results and the exact natural frequencies and also those found by using the classical Finite Elements Method (FEM). The first six natural frequencies (f_i, $i = 1, 2, \ldots, 6$, in rad/sec), for cantilevered conditions, are presented in *table II*.

The "exact" natural frequencies, presented in *table II* are found by employing the Dynamic Stiffness Matrix (DSM) presented in reference [2], and the results are verified by those given in reference [11].

The classical FEM's results, in this example, are first calculated from the finite beam element presented in reference [8]. Then, the tests were repeated with the beam element presented in reference [14]. The static stiffness matrix, in both cases, was found using the cubic "Hermite" type and linear approximations for flexural and torsional displacements, respectively. The mass matrix, for the former element [8], was calculated using linear approximations for all variables and for the latter element [14], it was obtained by using the cubic "Hermite" type and linear approximations for bending and torsion, respectively. The presented results are found when the beam is broken into 200 elements of equal length. As it can be seen, the natural frequencies, calculated by the first classical beam element, converge to values which are slightly different from the exact results. The error, in this case, is found to be up to 0.74 per cent (for the fourth natural frequency) whereas similar tests for the beam element of reference [14] and also the DFE showed very good convergencies (the corresponding results of *table II* are found when only six DFEs are used).

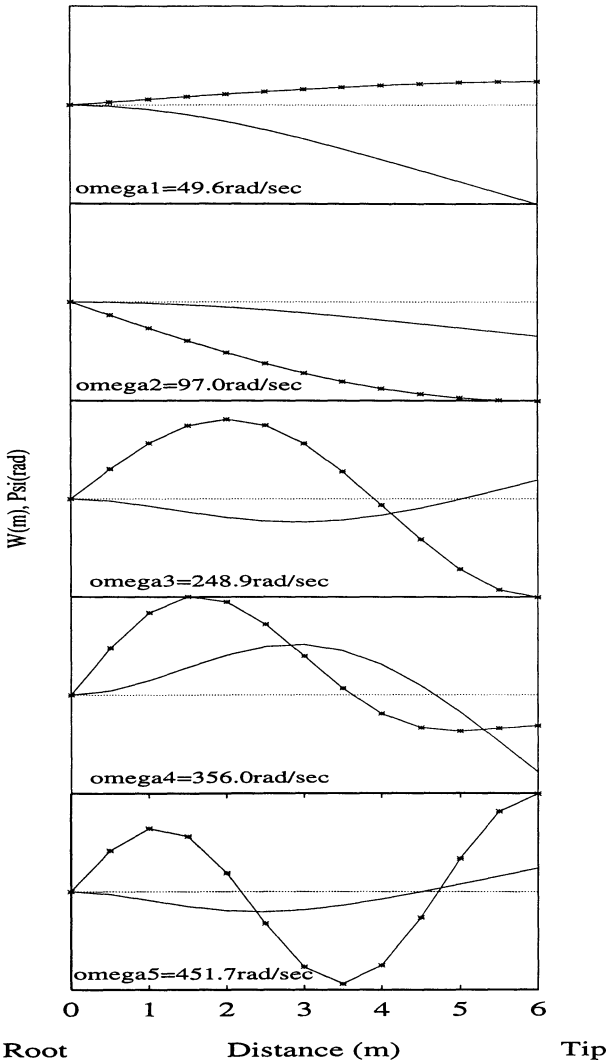

Figure 10. The coupled bending-torsional natural frequencies and mode shapes of an aircraft wing. ——, flexural displacement (W (m)); —∗—, torsional rotation (Ψ (rad)).

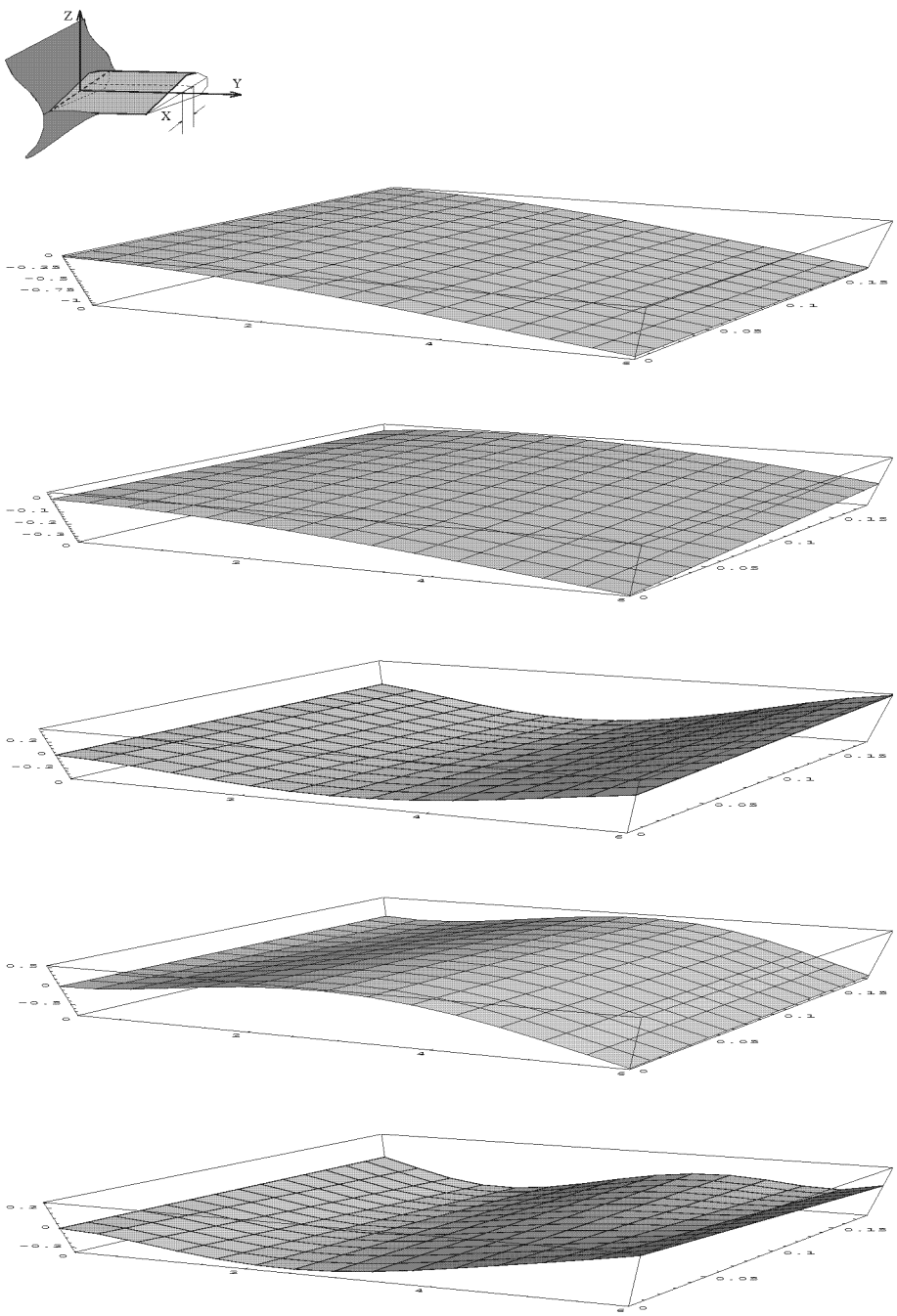

Figure 11. 3-D presentation of the first five Modes for a Bending-Torsional Coupled Airplane Wing.

When calculating the natural frequencies by the DFE method, j_m (the number of natural frequencies of beam element, still lying between zero and any trial ω, when all end displacements are assumed to be zero, in the Wittrick–Williams algorithm) was calculated in two different ways. First, j_m was calculated by the proposed method in this paper where $\Delta = D_f * D_t = 0$ (see equations (G), (H) in Appendix), and secondly, the calculations were repeated when j_m was found from "exact" expressions presented by Banerjee and Williams [5]. For this example, as for the other examples of this paper, identical results were found by both methods.

The convergency tests, made for the first five clamped-free (C-F) natural frequencies, obtained by the DFE

method are presented in *figure 8*. As it can be seen for the first three natural frequencies the error is found to be approximately zero ($\varepsilon \leqslant 0.1\%$), even when only four elements are used. For the fourth and fifth natural frequencies, the results are converging between $NE = 4$ and $NE = 6$ with less than 1 percent error.

Figure 9 shows the comparison between the convergency rates, for the first three clamped-free (C-F) natural frequencies, obtained from the classical FEM and the DFE method. Much better results were found by the DFE method.

The first five natural modes of this wing are shown in *figure 10*. *Figure 11* shows an illustration of these modes in 3-D. The natural frequencies are well separated, but the generated modes show substantial coupling between flexural displacement and torsional rotation.

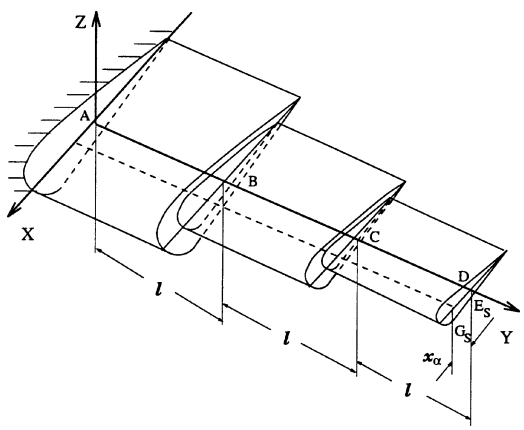

Figure 12. Coordinate system and notations for a straight three-beam airplane wing: E_s shear centre; G_s mass centre.

4.3. A typical three-beam aircraft wing

To illustrate the application of the DFE method to a more complex case, with variable geometry and mechanical properties, one can consider the cantilevered three-beam wing shown in *figure 12*. Segment lengths are chosen as $L_{AB} = L_{BC} = L_{CD} = l = 2$ m. The parameters for segment AB (taken from references [14,13,11]) are identical to the parameters of the first example. Each of segment *BC*'s parameters is two-thirds of segment *AB*'s value, and each of segment *CD*'s parameters is one-third of segment *AB*'s value. The first five natural frequencies calculated by the DFE method are given in *table III*, together with the exact results obtained by the DSM method [2], and the values with two different types of classical beam elements [14,8].

According to the results, the rates of convergence for the DFE were found to be about four times those found from the beam element presented in reference [8]. In other words, to find the same results as those obtained by the DFE method (in *table III*), the wing would have to be discretized with 24 static beam elements. The mass matrix, in this case, was obtained by using linear approximations for all variables. The same tests were repeated with the beam element presented in reference [14] where the mass matrix was obtained by using the cubic "Hermite" type and linear approximations for bending and torsion, respectively. For the first natural frequency, this element leads to much better precision compared to finite beam element of reference [8]. Moreover, both of these elements lead to approximately the same average error, evaluated for all of the five natural frequencies. The natural frequencies in *table III* calculated by the classical FEM follow the standard pattern of becoming progressively less accurate for higher modes.

Table III. Coupled bending-torsional Clamped-Free natural frequencies of a straight three-beam airplane wing.

	Frequency f_i [rad/sec]						
i	Exact[a]	DFE[b]	$\lvert\text{Err.}_{(b)}\rvert$	FEM[c]	$\lvert\text{Err.}_{(c)}\rvert$	FEM[d]	$\lvert\text{Err.}_{(d)}\rvert$
1	74.43	74.45	0.03(%)	74.27	0.22(%)	74.44	0.03(%)
2	128.57	128.61	0.03(%)	128.62	0.04(%)	128.69	0.09(%)
3	253.40	253.50	0.04(%)	254.75	0.53(%)	254.68	0.51(%)
4	376.59	378.35	0.47(%)	378.37	0.47(%)	378.74	0.57(%)
5	431.29	433.46	0.50(%)	435.27	0.92(%)	435.89	1.07(%)

[a] Each segment is modeled by one element of "exact DSM" type [2,3] (a total of 3 elements are used).

[b] Each of segments is divided into two equal DFEs (a total of 6 elements).

[c] The results obtained when each segment is modeled by four static beam elements [8] (number of total elements is 12).

[d] The results obtained when each segment is modeled by four static beam elements [14] (number of total elements is 12).

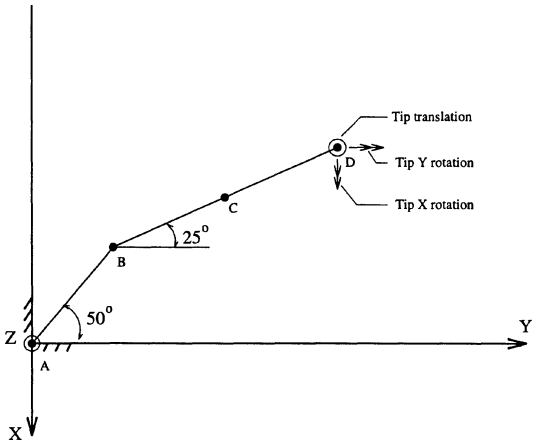

Figure 13. Elastic axis of a cantilevered planar three-beam wing, planform view.

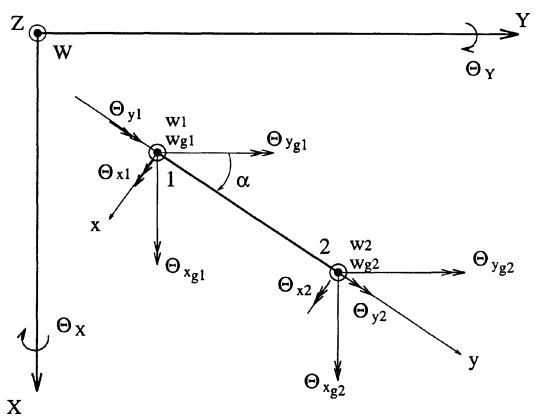

Figure 14. Elastic axis of beam element, with local (x–y) and global (X–Y) axes, and with degrees of freedom in local and global directions.

4.4. Natural frequencies of a planar wing

Another interesting case is the cantilevered three-beam assemblage illustrated in *figure 13*. This model represents an airplane wing with an elastic axis in coplanar straight-line segments [14]. Segment lengths and the parameters for all three segments are assumed to be as the preceding example. Having the element local matrix, equations (35) through (39), one next calculates a structure dynamic stiffness matrix by applying the standard assembling procedure of the FEM. For the planar assemblage, first, element local equation (35 through 39) is cast into global form by the standard geometric transformations [14,8] (see *figure 14* which illustrates the degrees of freedom of the beam element in two different coordinate system). Next, the element global matrices of all beams in the structure are superimposed appropriately to form the unrestrained structure matrix which, in turn, is changed to the global stiffness matrix of the structure by accounting for the boundary conditions. Employing this procedure,

Table IV. Coupled bending-torsional natural frequencies of a typical planar wing.

	Natural frequencies; f_i [rad/sec]		
i	Exact[a]	DFE[b]	$\lvert\text{Error}_{DFE}\rvert$(%)
1	65.03	65.05	0.015
2	129.78	129.79	0.008
3	244.11	244.31	0.082
4	396.24	396.60	0.091
5	441.95	446.19	0.959

[a] Each segment is modeled by one element of "exact DSM" type [2,3](a total of 3 elements).

[b] Each of segments is divided into two equal DFEs (a total of 6 elements).

the exact natural frequencies together with the DFE method's results of the planar wing (*figure 13*), are calculated and are shown in *table IV*. The exact results are calculated, as in the previous examples, by the DSM method [2] when each segment is modeled by only one beam element. To obtain the natural frequencies due to the DFE method each segment is broken into two beam elements and excellent agreements were found between these results and the exact natural frequencies.

5. Concluding remarks

In summary, a Dynamic Finite Element (DFE) has been developed and illustrated for the calculation of natural frequencies and modes of straight uniform beams with non-coincident elastic and inertia axes, and simple planar assemblies of such beams. The application of the methodology was investigated by free vibration analysis of a variety of examples such as an open-box section beam of different boundary conditions (i.e., clamped-clamped (C-C), clamped-free (C-F) and simply supported-simply supported (SS-SS)). A group of different configurations of closed-section beam-like uniform and non-uniform straight and planar wings are also studied. The results of the DFE, for all the cases studied here, agree very well with those obtained from the "exact" DSM approach and comparing with the FEM, higher convergency rates were obtained when compared to the DFE method. The general approach presented earlier by the authors (see [16,17,19]), can be exploited to extend the present formulation to more complex cases such as non-uniform coupled beams. On the other hand, it will be possible to take into account the effects of shear deformation and rotary inertia, which are significant for beams having large cross-sectional dimensions in comparison to their length and also when higher modes are important [4]. We note in closing that the DFE method can be used for the vibrational analysis of beam assemblage with attached rigid members [1]. Thus, the DFE stiffness matrix derived

here provides also a basis for analysis of a beam model of a complete aircraft carrying essentially rigid masses such as engines and missiles.

Acknowledgments

Special thanks are due to Professor G. Dhatt, from l'INSA de Rouen (France), for valuable comments and scientific discussions. The authors wish to acknowledge the scholarship awarded by the Ministry of Culture and Higher Education (MCHE) of Iran which made this work possible. The authors are also grateful to the Natural Sciences and Engineering Research Council of Canada (NSERC) which also supported this research.

Appendix. Dynamic shape functions

$$N_1(\omega)_f = \left(\alpha^2\right) * \left\{-\cos(\alpha\xi) + \cos\left(\alpha(1-\xi)\right) * \cosh\alpha + \cos\alpha * \cosh\left(\alpha(1-\xi)\right) - \cosh(\alpha\xi) - \sin\left(\alpha(1-\xi)\right) * \sinh\alpha + \sin\alpha * \sinh\left(\alpha(1-\xi)\right)\right\}/D_f, \quad \text{(A)}$$

$$N_2(\omega)_f = (\alpha) * \left\{\cosh\left(\alpha(1-\xi)\right) * \sin\alpha - \cosh\alpha * \sin\left(\alpha(1-\xi)\right) - \sin(\alpha\xi) + \cos\left(\alpha(1-\xi)\right) * \sinh\alpha - \cos\alpha * \sinh\left(\alpha(1-\xi)\right) - \sinh(\alpha\xi)\right\}/D_f, \quad \text{(B)}$$

$$N_3(\omega)_f = \left(\alpha^2\right) * \left\{-\cos\left(\alpha(1-\xi)\right) + \cos(\alpha\xi) * \cosh\alpha - \cosh\left(\alpha(1-\xi)\right) + \cos\alpha * \cosh(\alpha\xi) - \sin(\alpha\xi) * \sinh\alpha + \sin\alpha * \sinh(\alpha\xi)\right\}/D_f, \quad \text{(C)}$$

$$N_4(\omega)_f = (\alpha) * \left\{-\cosh(\alpha\xi) * \sin\alpha + \sin\left(\alpha(1-\xi)\right) + \cosh\alpha * \sin(\alpha\xi) - \cos(\alpha\xi) * \sinh\alpha + \sinh\left(\alpha(1-\xi)\right) + \cos\alpha * \sinh(\alpha\xi)\right\}/D_f, \quad \text{(D)}$$

$$N_1(\omega)_t = \cos(\tau\xi) - \cos\tau * \sin(\tau\xi)/D_t, \quad \text{(E)}$$

$$N_2(\omega)_t = \sin(\tau\xi)/D_t, \quad \text{(F)}$$

and

$$D_f = \left(\alpha^2\right) * \left\{-2 * (1 - \cos\alpha * \cosh\alpha)\right\}, \quad \text{(G)}$$

$$D_t = \sin\tau. \quad \text{(H)}$$

References

[1] Åkesson B., PFVIBAT – A computer program for plane frame vibration analysis by an exact method, Int. J. Numer. Meth. Eng. 10 (1976) 1221–1231.

[2] Banerjee J.R., Coupled bending-torsional dynamic stiffness matrix for beam elements, Int. J. Numer. Meth. Eng. 28 (1989) 1283–1298.

[3] Banerjee J.R., Fisher S.A., Coupled bending-torsional dynamic stiffness matrix for axially loaded beam elements, Int. J. Numer. Meth. Eng. 33 (1992) 739–751.

[4] Banerjee J.R., Williams F.W., Coupled bending-torsional dynamic stiffness matrix for Timoshenko beam elements, Comput. Struct. 42 (3) (1992) 301–310.

[5] Banerjee J.R., Williams F.W., Clamped-clamped natural frequencies of a bending-torsion coupled beam, J. Sound Vib. 176 (3) (1994) 301–306.

[6] Bathe K.J., Finite Element Procedure in Engineering Analysis, Prentice-Hall, Englewood-Cliffs, NJ, 1982.

[7] Batoz J.-L., Dhatt G., Projet RE-FLEX: (Recherche et Enseignement en modélisation des structures FLEXible), Division MNM/Département GM, Université de Technologie de Compiegne, France.

[8] Batoz J.-L., Dhatt G., Modélisation des structures par éléments finis, Vol. 2: poutres et plaques, Hermès, Paris et Les presses de L'Université Laval, Québec, 1990.

[9] Bisplinghoff R.L, Ashley H., Halfman R.L., Aeroelasticity, Addison-Wesley, Reading, MA, 1955.

[10] Dhatt G., Touzot G., Une présentation de la méthode des éléments finis, Maloine S.A., Paris et Les presses de L'Université Laval, Québec, 1981, pp. 100–103.

[11] Eslimi-Isfahani S.H.R., Banerjee J.R., Sobey A.J., Response of a bending-torsion coupled beam to deterministic and random loads, J. Sound Vib. 195 (2) (1996) 267–283.

[12] Fung Y.C., An Introduction to The Theory of Aeroelasticity, Dover Publications, New York, 1969.

[13] Goland M., Flutter of a uniform cantilever wing, J. Appl. Mech. 12 (1945) A197–A208.

[14] Hallauer W.L., Liu R.Y.L., Beam bending-torsion dynamic stiffness method for calculation of exact vibration modes, J. Sound Vib. 85 (1982) 105–113.

[15] Hashemi S.M., Richard M.J., On the coupled bending-torsional natural frequencies and modes of beams; A frequency dependent Dynamic Finite Element (DFE), in: Proceedings of Canadian Society for Mechanical Engineering (CSME) Forum 1998, Ryerson Polytechnic University, Toronto, Ontario, Canada, May 19–22, 1998, pp. 468–475.

[16] Hashemi S.M., Richard M.J., Dhatt G., A Bernoulli–Euler stiffness matrix approach for vibrational analysis of linearly tapered beams, in: Proceedings of Acoustics Week in Canada 1996, Calgary, Alberta, 87, October 7–11, 1996.

[17] Hashemi S.M., Richard M.J., Dhatt G., A Bernoulli–Euler stiffness matrix approach for vibrational analysis of spinning linearly tapered beams, 42nd ASME Gas Turbine and Aeroengine Congress, Orlando, Florida, June 2–5, 1997, Paper No. 97-GT-500.

[18] Hashemi S.M., Richard M.J., Dhatt G., A Dynamic Finite Element (DFE) formulation for free vibration analysis of centrifugally stiffened uniform beams, in: Proceedings of 16th CANadian Congress of Applied Mechanics (CANCAM 1997), Québec, June 1–6, 1997, pp. 443–444.

[19] Hashemi S.M., Richard M.J., Dhatt G., A New Dynamic–Finite Element (DFE) formulation for lateral free vibrations of Euler–Bernoulli spinning beams using trigonometric shape functions, J. Sound Vib., to be published.

[20] Hurty W.C., Rubinstein M.F., Dynamic of Structures, Prentice-Hall, Englewood Cliffs, NJ, 1964.

[21] Mei C., Coupled vibrations of thin-walled beams of open-section using the finite element method, Int. J. Mech. Sci. 12 (1970) 883–891.

[22] Swannell P., The automatic computation of the natural frequencies of structural frames using an exact matrix technique, in: Theory and Practice in Finite Element Structural Analysis, University of Tokyo Press, 1973, pp. 289–304.

[23] Williams F.W., Wittrick W.H., An automatic computational procedure for calculating natural frequencies of skeletal structures, Int. J. Mech. Sci. 12 (1970) 781–791.

[24] Wittrick W.H., Williams F.W., A general algorithm for computing natural frequencies of elastic structures, Q. J. Mech. Appl. Math. 24 (1971) 263–284.

[25] Wittrick W.H., Williams F.W., On the free vibration analysis of spinning structures by using discrete or distributed mass models, J. Sound Vib. 82 (1) (1982) 1–15.